

Article

Insight of Numerical Simulation for Current Circulation on the Steep Slopes of Bathymetry and Topography in Palu Bay, Indonesia

Mohammad Lutfi

Department of Petroleum Engineering, STT MIGAS, Balikpapan 76127, Indonesia; lutfi_plhld@yahoo.co.id

Abstract: The steep slope of the bathymetry and topography that surrounds Palu Bay is a unique morphology of the area that affects the currents. A simulation was carried out in three regions with seven scenarios to understand the effect of wind, tide, and discharge on currents. The results showed that the average current pattern in Palu Bay is more dominantly influenced by tides at the open boundary and in the middle of the bay, steered by wind directions. The velocity decreases when it reaches the end of the bay and eventually reverses back to the mouth of the bay through both sides of the bay. The current in the Palu River estuary with a discharge of $36 \text{ m}^3/\text{s}$ moves out of the river mouth. On the other hand, results with a discharge of $2 \text{ m}^3/\text{s}$ revealed that the tidal current in the middle layer to the lower layer moves in the opposite direction to the current generated by the discharge in the layer above. It means that the tidal current velocity is lower than that generated by the river discharge. The computation revealed a good agreement with observed current velocity at the selected observation points.

Keywords: numerical modeling; current; steep slopes; bathymetry; topography; Palu



Citation: Lutfi, M. Insight of Numerical Simulation for Current Circulation on the Steep Slopes of Bathymetry and Topography in Palu Bay, Indonesia. *Fluids* **2021**, *6*, 234. <https://doi.org/10.3390/fluids6070234>

Academic Editors: Amparo López Jiménez and Modesto Pérez-Sánchez

Received: 13 May 2021
Accepted: 25 June 2021
Published: 29 June 2021

Publisher's Note: MDPI stays neutral with regard to jurisdictional claims in published maps and institutional affiliations.



Copyright: © 2021 by the author. Licensee MDPI, Basel, Switzerland. This article is an open access article distributed under the terms and conditions of the Creative Commons Attribution (CC BY) license (<https://creativecommons.org/licenses/by/4.0/>).

1. Introduction

Palu Bay is located on the west coast of Sulawesi Island, which is in the province of Central Sulawesi, Indonesia (see Figure 1). The bay is a shipping lane, where there are several ports that play a role in reviving and developing the regional economic sector. The capital of Central Sulawesi Province is Palu City [1]. The southern part of the bay is an estuary [2], and the surrounding area is a popular tourist attraction and commercial (e.g., malls and restaurants) [3] spot.

Palu Bay is surrounded by a series of high mountains [4] in the shape of a bowl with an altitude of more than 500 m above the sea level (masl). The elevation of the hill in Mantantimali reaches up to 1500 masl. The location, altitude, temperature, and wind conditions are very conducive for paragliding. This hill is one of the best paragliding locations in the Southeast Asia and even in the world [5]. In addition, Palu Bay border with the Makassar Strait. These factors strengthen the wind gusts in the bay.

Recently, hydrodynamic numerical models have become the center of attention by researchers for the investigation of the Palu, Sigi, and Donggala (Pasigala) disaster on 28 September 2018 at 18:02:44 local time (10:02:44 UTC). It was triggered by an earthquake with the epicenter at 0.18° S and 119.85° E , Central Sulawesi, Indonesia [6]. This disaster was the deadliest natural disasters throughout 2018. This resulted in thousands of deaths [7] and infrastructure damage such as houses, public facilities and transportation routes [8]. Field observations at the four ports in Palu Bay, namely the ports of Wani, Pantoloan, Taipa, and Donggala, revealed that several ships were stranded on land, whereas one of them weighing 500 tons was dragged about 80 m ashore [9].

Many studies related to tsunami numerical modeling to investigate the causes and impacts of the disaster have been published [10–12], etc. One of the uniqueness of this disaster is that the cause is not directly related to the strike slip earthquake, since this

mechanism rarely generates a tsunami [13]. Seabed sediment landslides due to earthquakes are the direct cause of tsunamis [14,15]. One of the causes of the instability of the seabed sediments during the earthquake is the steep slopes of bathymetry. It is proven that the water depth that rapidly changes near the coastline and it gets steeper into the middle of the bay based on the Global Bathymetric Data of the General Bathymetric Chart of the Ocean (GEBCO) [16].

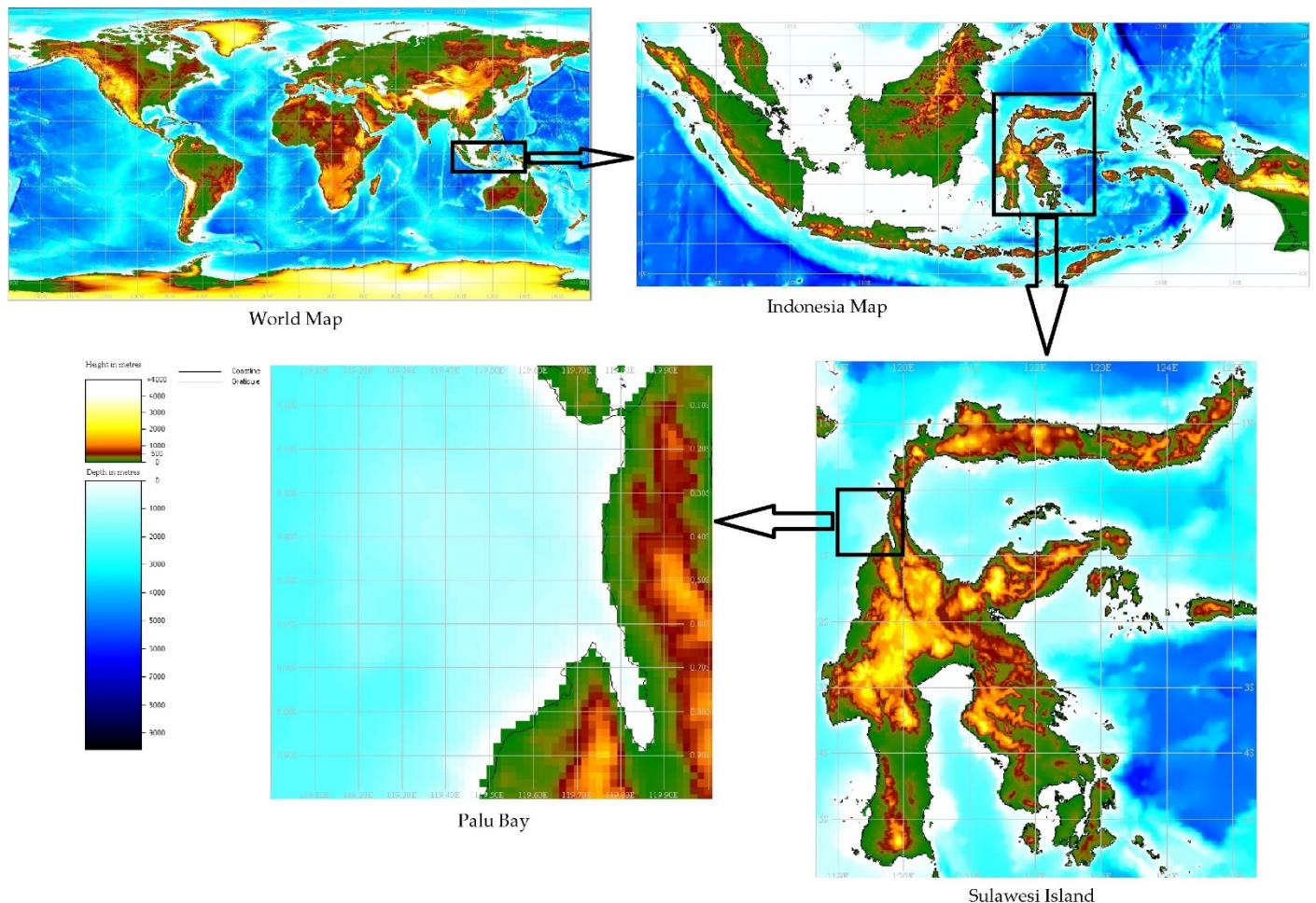


Figure 1. Location of Palu bay, Sulawesi island, Indonesia on the world map (source: GEBCO).

The steepness of the topography and bathymetry in this area are two important factors that influence the current movement pattern and the velocity. Numerical models are needed to represent events in the past (e.g., disaster investigation), the present (e.g., early warning systems), and the future (e.g., future development planning). Therefore, the results of this study are expected as an insight for stakeholders to develop the Palu Bay and vicinity with an environmental perspective that is responsive to disasters.

2. Methods

This model was built to analyze the water current movement in Palu Bay which is influenced by wind, tide, and river discharge. The three components are used as input data for the model separately to understand the effect of each component on the dynamics of current movement. The simulation is also carried out by combining several components to understand which component is more dominant.

Estuary Coastal Ocean Model and Sediment Transport (ECOMSED) developed by Hydroqual [17] is used for hydrodynamic modeling. This model was developed based on the Princeton Ocean Model (POM) [18]. It uses finite difference methods by applying

a sigma coordinate system to vertical cross sections. The system depends on the bottom of the water based on transformation [19] to analyze the physical processes that occur in the vertical layer. Wind data was used at the surface boundary. This data is obtained from the Meteorological, Climatological, and Geophysical Agency (BMKG), where the wind vector on land is transformed into a wind data vector with a height of 10 m above sea level (U_{10}) [20]. Coastline and riverbank coordinates obtained from google earth imagery was imposed at closed boundary (areas bordering land). Tidal data was imposed at the open boundary at the mouth of the bay. Meanwhile river depth obtained from the Public Works office of Palu City and bathymetry obtained from the Hydrographic and Oceanographic Center, Indonesian Navy (PUSHIDROSAL) were used at the bottom boundary by interpolating the contours on the sea map and the sketch of a cross section of the river.

The boundaries of the research area in geographic coordinates are as follows: $119^{\circ}43'42''$ western most longitude, $119^{\circ}52'58''$ eastern most longitude, $0^{\circ}35'3''$ northern most latitude, and $0^{\circ}53'12''$ southern-most latitude. The simulation area consists of three models covering the entire Palu bay (model I), a small part of the Palu river estuary (model II), and the mouth of the Palu river (model III). Each model consists of several simulations with certain scenarios.

Model I consists of three simulations, where the first and second simulations were carried out separately using wind and tides as generating forces. The third simulation was conducted by combining the effects of wind and tides for one month simultaneously. The output is the monthly average current direction and its velocity.

The stability test for model I was carried out by assuming that the bay conditions are considered uniform. In this condition, the depth, tidal conditions, and wind that blow over the water surface are considered constant for each grid. Furthermore, the stable simulation results in the previous stage are used as the initial conditions in the next stage simulation. At this stage, the current generating forces are no longer considered uniform. Wind and tidal data with 1 h intervals were used during simulation. This computation was run with horizontal finite difference meshes are 126×63 grids.

Model II uses tides and discharge of $2 \text{ m}^3/\text{s}$ and $36 \text{ m}^3/\text{s}$ as generating forces to analyze the influence of small and large discharge on current movements in the estuary. This simulation was run on a horizontal section with horizontal finite difference meshes are 125×125 grids and vertically discretized with 11 σ -levels. Meanwhile, model III is a nested model to model II. The initial conditions of this model use the output of model II as input data. It was built to increase the resolution in the delta and vicinity at the mouth of the river with the same scenario as model II. Initial conditions for both models were obtained from observation data of temperature, salinity, river discharge, and tide. The initial and boundary conditions for salinity and temperature are assumed to be constants 0 ppt and 28°C at the river upstream and 30 ppt and 29°C at the sea respectively.

A Floater Current Meter connected to a GPS was used to measure the velocity and direction of the current for model verification. Data were taken at two locations, namely, Pantoloan Port and at the mouth of the Palu River. This measurement was conducted at low slack, low slack, high slack, and highest water conditions in both locations.

3. Results and Discussion

3.1. Large Model

The effect of wind, tide, and the combination of these two components on the current circulation is discussed in this section. The river discharge has not been included in this model because the width of the Palu river which empties into the Palu Bay is very small compared to the size of the Palu Bay. A high spatial horizontal resolution is required so that the Courant–Friedrich–Levy (CFL) criteria are met. The effect of river discharge will be discussed in the small model through a separate simulation.

3.1.1. Wind Patterns Palu Bay

The wind that enters Palu Bay originates from the north of the Philippines and then enters the Makassar strait. It divides into two and one branch enters Palu Bay which is narrower than the Makassar strait. The maximum value of wind velocity in the Makassar strait in the east monsoon is more than 4.5 m/s [21]. The topography around Palu Bay causes mountain winds to blow from the west and east sides of the bay. The wind that blows on the surface of Palu Bay waters is focused and blows faster than the surrounding area (areas affected by global climate). Figure 2 shows the wind class frequency distribution for wind velocity and its direction in September measured at BMKG station in Palu City.

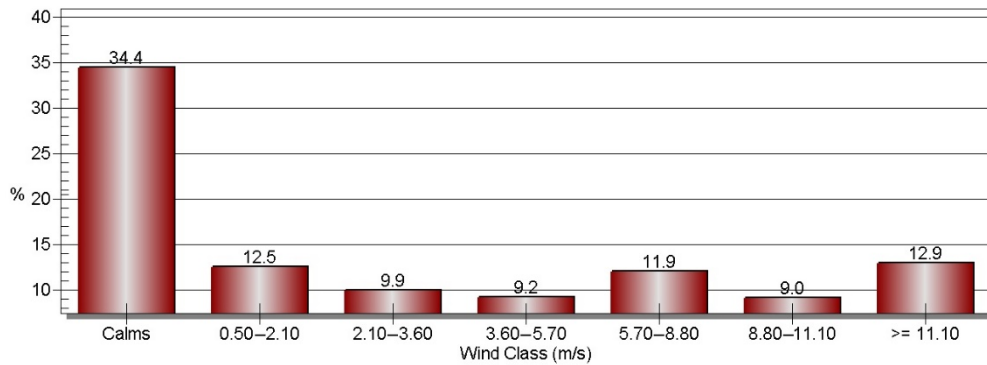


Figure 2. Wind class frequency distribution.

It can be seen in Figure 2 that the most dominant wind velocity other than calm condition occurs at a velocity above 11.10 m/s with a percentage of 12.9%. This means that the average wind velocity blowing in Palu Bay is stronger than the wind that blows in the Makassar strait with the highest velocity intervals of 5.14 m/s to 7.71 m/s in September [22]. The prevailing wind occurs in the north with a percentage of 7.3% based on the wind rose (Figure 3).

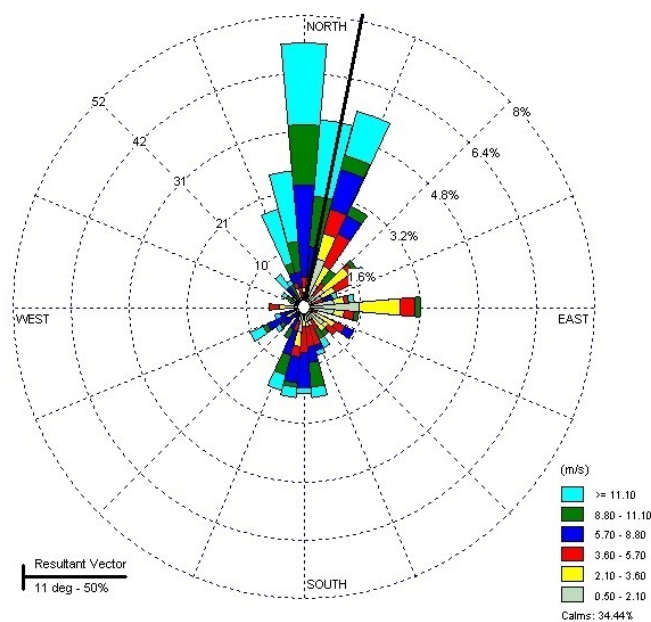


Figure 3. Wind rose in Palu City.

3.1.2. Model of the Average Sea Surface Current Generated by Wind

It has been understood based on previous research [23] that there are complex non-linear interactions and energy transfers between ocean wind-waves and the mean flow.

Surface winds can affect surface currents [24]. The Coriolis force causes the current to turn perpendicular to the direction of the wind [25]. However, the deflection caused by the Coriolis effect is so small in Palu Bay because the location of the bay is close to the Equator and narrow. It reveals that surface currents are more dominantly influenced by the local wind system that blows over the water surface. This is consistent with previous research [26], where the Coriolis effect of the Earth disappears so that the current moves in the direction of the wind [27].

Prevailing wind reveals that the dominant wind direction blows from the north based on wind rose (Figure 3). This is in line with the simulation result (Figure 4a) which show that the average current pattern in one month moves from the open boundary (northern part) into the middle of the bay with a maximum velocity of 0.73 m/s. The velocity decreases when it reaches the end of the bay and eventually reverses towards the mouth of the bay through both sides. The reversal is caused by wind deflection due to the steep slopes of topography around the bay. Meanwhile, the decrease in velocity is caused by the narrowing of the bay due to the steep slopes of bathymetry. The simulation result (Figure 4a) reveals that the velocity in the middle of the bay is faster than the shallow waters along the coast. This result is supported by previous studies that reported that Palu Bay bathymetry has a parabolic cross-sectional shape [28,29].

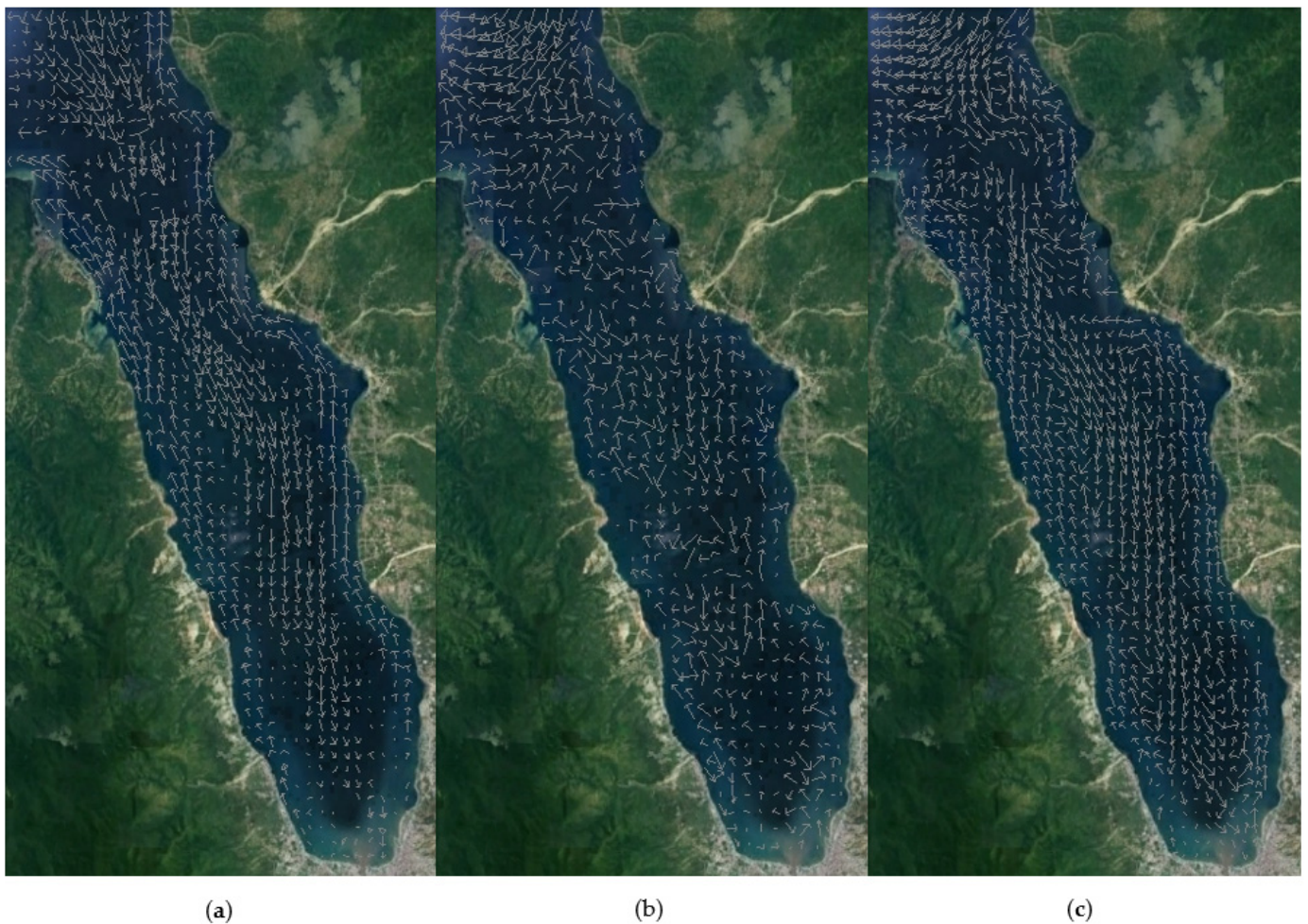


Figure 4. The average of ssa surface current pattern for model I (a) generated by wind; (b) generated by tide; and (c) generated by wind and tide.

3.1.3. Model of the Average Surface Currents Generated by the Tides

Current movements in the bay, in general, are more dominantly influenced by tides [30–32]. The simulation result (Figure 4b) show that tidal currents at a relatively high velocity occur only in the open area with a maximum velocity of 1.37 m/s. In this area some of the currents originating from the north enter the bay while others turn westward. From the western part in the open area the currents enter the bay at a velocity of less than 0.5 m/s, where there are no reversed currents in the area bordering the land (closed boundary area). This model does not include the influence of wind as input data, so there is no current deflection along the coast.

3.1.4. The Average Sea Surface Current Generated by Tides and Winds

The simulation results (Figure 4c) show that the current pattern in Palu Bay is more dominantly influenced by tides at the open boundary with a maximum velocity of 1.5 m/s. It can be seen that the current with high velocity occurs at the mouth of the bay in an area with open boundary with the dominant current coming from the north. This is caused by pressure from the Indonesian throughflow (ITF) system [33–35]. The flow is a transportation route that connects the northern equator of the Pacific Ocean directly with the Indian Ocean. The currents from Mindanao flows into the Sulawesi sea towards the Kalimantan coast, and then join other currents coming from the south China sea [36,37]. Meanwhile, in the middle of the bay the current pattern follows the current pattern generated by the wind. It reveals that as a whole the current movement in the bay is dominated by the influence of the wind.

3.2. Small Model

There are many small rivers that empty into Palu Bay. However, the Palu River is the largest one among them. Therefore, this model only focuses on the Palu River estuary. Due to the lack of river depth data, the domain model II only covers a small part of the estuary, namely a small part of the bay and a small part of the river.

A high horizontal grid resolution is required to make the model domain cover the entire bay and estuary. But this is difficult to do, since the comparison between the horizontal grid size and the maximum depth in the model domain will be large, and the CFL criterion cannot be satisfied which will cause a run time error [38]. The high resolution covering Palu Bay and Palu River is also not sufficient to describe the real situation. The position of the delta in the middle of the river mouth causes the river flow to be divided in two directions, namely to the east and west. Therefore, the increase in resolution in the delta area is carried out in model III.

3.2.1. Surface Current with Discharge as Generating Force

The direction of current movement at high slack water and low slack water conditions are opposite each other [39,40]. The maximum tidal flow velocity is reached under these conditions. From the simulation results (Figure 5), the direction of movement of surface currents when the maximum tidal current velocity moves out of the river mouth. This reveals that the influence of river discharge of $36 \text{ m}^3/\text{s}$ is more dominant than the effect of tidal currents. The maximum velocity of the current at high slack water is 0.47 m/s smaller than at low slack water with a maximum speed of 0.53 m/s. At high slack water, the tidal currents move into the river so that the direction of the river flow from the upstream is opposite to the direction of the tidal currents. This condition weakens the flow from upstream. Meanwhile, at low slack water condition, the direction of tidal currents moves in the same direction as the river flow from the upstream so that the resulting currents amplify each other.

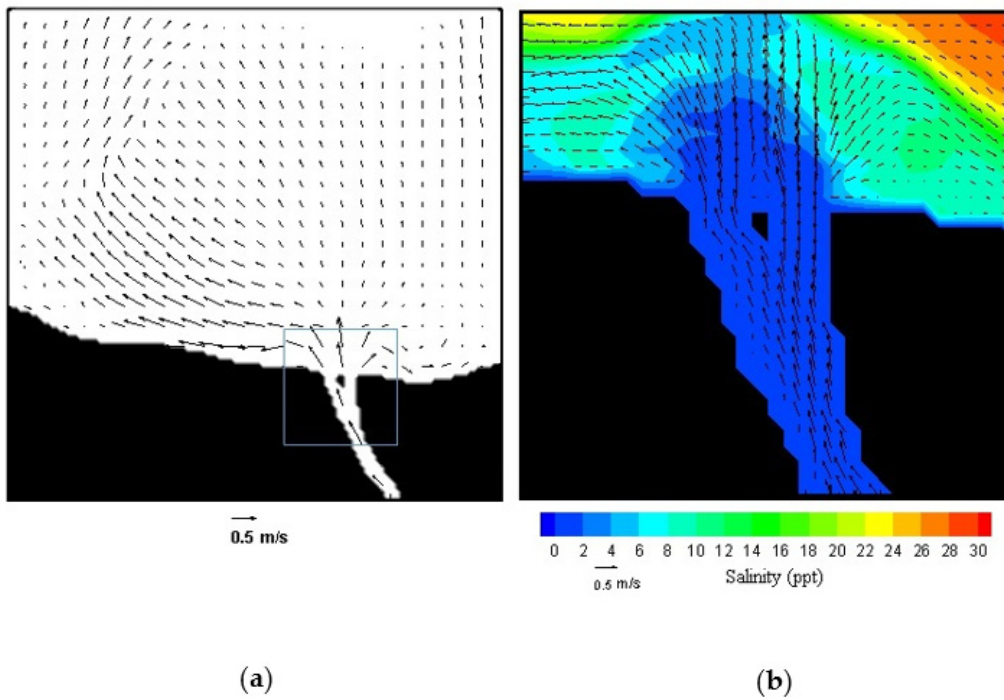


Figure 5. Current pattern at high slack water condition (a) model II and (b) model III.

The location of the delta in the middle of the river mouth causes the current to spread west and east after the current passes through the delta. The simulation results (Figure 6) show that the currents generated by the tides and the discharge move at a higher velocity to the west, then weaken towards the north due to changes in depth. The current velocity is greater in the deeper area compared to the surrounding area. Depth degradation causes the flow to form eddies by slowing current velocity due to friction at the bottom of the water and increasing current velocity by silting waters [41,42].

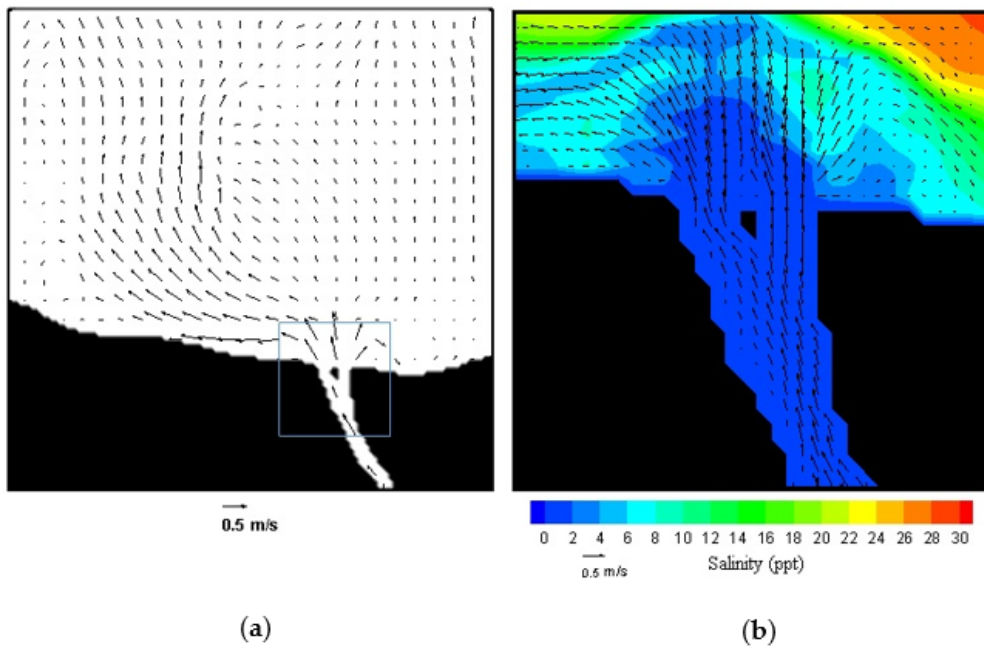


Figure 6. Current pattern at low slack water condition (a) model II and (b) model III.

3.2.2. Current Circulation on Vertical Cross Section

The simulation results for a discharge of $36 \text{ m}^3/\text{s}$ (Figure 7) show that the current moves out of the river at all layers. The current velocity decreases from surface to bottom. This is caused by the current velocity being decelerated by friction with the bottom of the water. This result is in line with the results of previous studies which state that the decrease in velocity is proportional to the increase in bottom friction [43].

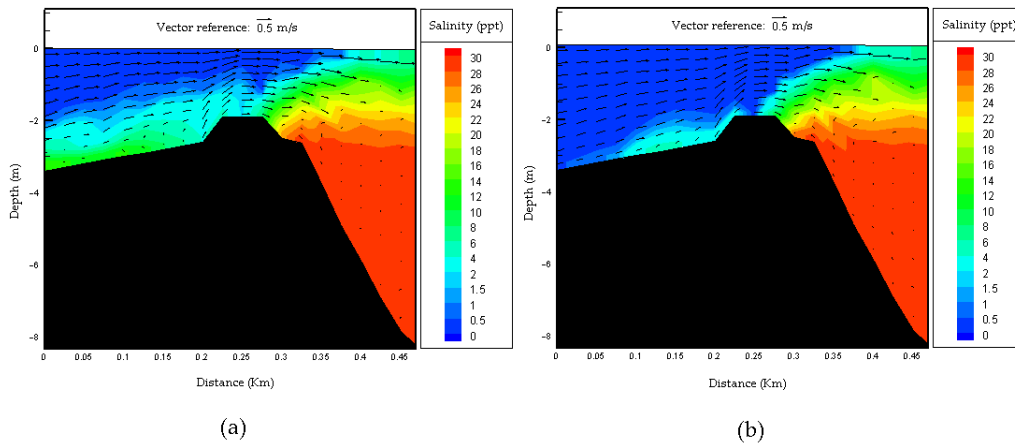


Figure 7. Current pattern on the vertical cross section for discharge of $36 \text{ m}^3/\text{s}$ (a) low slack water condition and (b) high slack water condition.

The simulation results with a discharge of $2 \text{ m}^3/\text{s}$ (Figure 8) show that the current velocity in layer 6 (σ_6) to layer 11 (σ_{11}) moves in the opposite direction to the current in the layer above. This shows that the current velocity at σ_6 to σ_{11} which is indicated by the sign (-) is influenced by the tidal currents entering the river. The simulation results reveal that river discharge dominates the direction of current movement from the upstream to the downstream.

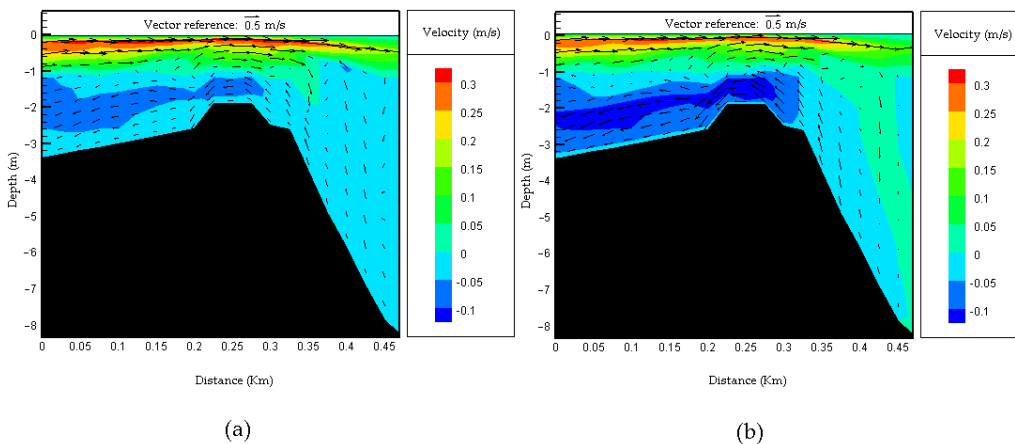


Figure 8. Current pattern on the vertical cross section for discharge of $2 \text{ m}^3/\text{s}$ (a) low slack water condition and (b) high slack water condition.

Current is a manifestation of the movement of water masses. The output of the current simulation can be used as input into the model on the water quality module in the ECOMSED program. One of the polluted rivers that empties into Palu Bay is the Poboya River. Massive use of Mercury in the illegal gold mine in the Poboya area has polluted the water of the Poboya river. Further research is expected to be able to model the dispersion of pollutants that accumulate in Palu Bay based on this model.

3.2.3. Verification

Figure 9a,b show a velocity-time graph for the simulation results and observations at the port of Pantoloan and at the mouth of the Palu River with a discharge of $2 \text{ m}^3/\text{s}$. It shows a similar pattern with the good root mean square error (RMSE) values of 0.01 m/s and 0.56 m/s , respectively. The RMSE value at the Pantoloan port was better than the RMSE value at the mouth of the Palu river. This is because the input of river depth data at the verification location obtained from the Public Works Office of Palu City is the result of interpolation from the sketch of a cross section of the river. The results of depth interpolation should not be used as input data in the model for verification purposes in the river mouth that experience high sedimentation dynamics. In order to obtain better simulation results at the verification location, the water depth observation data at the verification points must be used as input data for the initial conditions of the simulation.

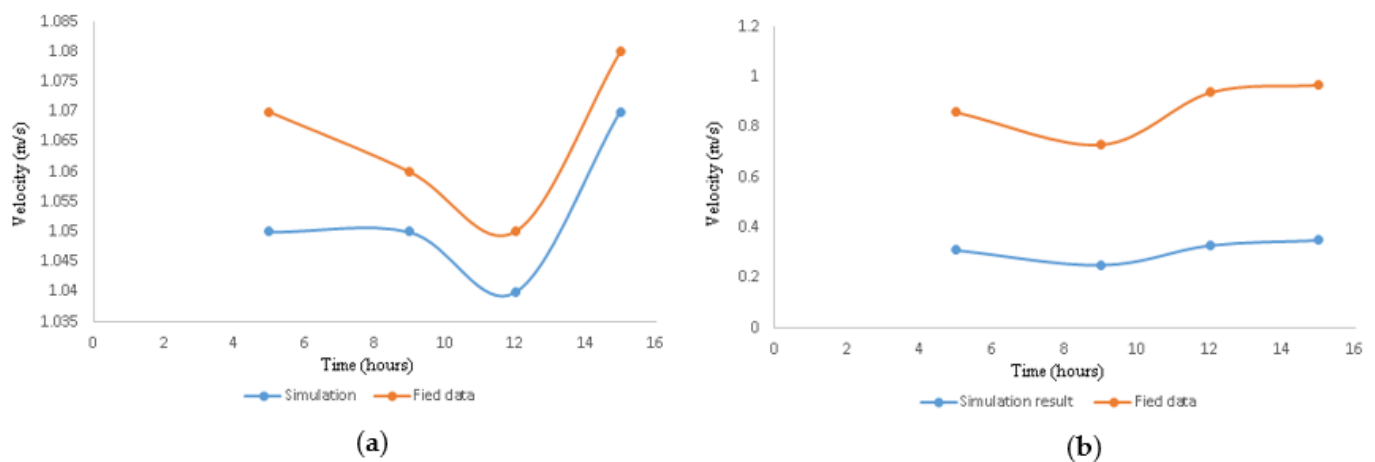


Figure 9. Verification of current velocity (a) Pantoloan port and (b) river mouth.

4. Conclusions

The simulation results revealed that the average current movement pattern in Palu bay is more dominantly influenced by tides at the open boundary with a maximum velocity of 1.7 m/s , whereas in the middle of the bay the current pattern follows the pattern generated by the wind. The velocity decreases when it reaches the end of the bay and it turns back towards the mouth of the bay through the two sides of the bay due to the steep slopes of the bathymetry and topography around the bay.

The movement of surface currents in the estuary of the Palu River with a river discharge of $36 \text{ m}^3/\text{s}$ moves out of the river mouth. Meanwhile, the simulation results with a discharge of $2 \text{ m}^3/\text{s}$ revealed that the tidal currents in the middle layer to the lower layer move in the opposite direction to the current generated by the discharge in the layer above, tidal current velocity is smaller than the current generated by discharge. It can be concluded that river discharge is more dominant in the estuary of the Palu river. The simulation result seems to be corresponding to observed current velocity with RMSE value of 0.01 m/s at the Pantoloan port and 0.56 m/s at the river mouth.

The bathymetry used in this study still uses data prior to the tsunami disaster caused by underwater landslides. It has been known from many previous studies that bathymetry in Palu Bay has undergone many changes since the incident. Therefore, updated bathymetry data is needed to rebuild the current model.

Funding: This research was supported by a grant from the STT MIGAS, with contract number 013/SP/Penelitian-LPPM/Desember/2020.

Institutional Review Board Statement: Not applicable.

Informed Consent Statement: Not applicable.

Data Availability Statement: Not applicable.

Acknowledgments: I would like to express my gratitude to International Development and Cooperation, Hiroshima University for the GIS software facility in the laboratory for the completion of several simulations. My special thanks go to Mardeli Jandja for the insight during his life.

Conflicts of Interest: The author declare no conflict of interest in this research.

References

1. Syifa, M.; Kadavi, P.R.; Lee, C.-W. An Artificial Intelligence Application for Post-Earthquake Damage Mapping in Palu, Central Sulawesi, Indonesia. *Sensors* **2019**, *19*, 542. [[CrossRef](#)] [[PubMed](#)]
2. Ifiginia; Pudyastuti, P.S.; Kuswartomo; Hidayati, N. The Analysis of Backwater Impact on the Increasing of Flood Water Level in Palu River. In *AIP Conference Proceedings*; AIP Publishing LLC: Melville, NY, USA, 2018; Volume 1977, p. 050007.
3. Paulik, R.; Gusman, A.; Williams, J.H.; Pratama, G.M.; Lin, S.L.; Prawirabhakti, A.; Sulendra, K.; Zachari, M.Y.; Fortuna, Z.E.D.; Layuk, N.B.P.; et al. Tsunami hazard and built environment damage observations from Palu City after the September 28 2018 Sulawesi earthquake and tsunami. *Pure Appl. Geophys.* **2019**, *176*, 3305–3321. [[CrossRef](#)]
4. Metzner, J. Palu (Sulawesi): Problematik der Landnutzung in einem klimatischen Trockental am Äquator (Palu (Sulawesi): Problems of Land Utilization in a Climatic Dry Valley on the Equator). *Erdkunde* **1981**, *35*, 42–54. [[CrossRef](#)]
5. Adrikni, W.K.M.; Akhmad, S.A.; Anjar, H.; Amalfi, O.; Asdani, S.A.C.; Defrizal, D.A.Y.R.; Firdaus; Fadli, G.M.; Lucky, D.G.H.; Haunan, A.; et al. *Bencana Melanda Geologi Menata*, 1st ed.; Badan Geologi Kementerian Energi dan Sumber Daya Mineral: Jakarta, Indonesia, 2018; pp. 2–3. ISBN 978-602-9105-76-6. (In Indonesian)
6. Gusman, A.R.; Supendi, P.; Nugraha, A.D.; Power, W.; Latief, H.; Sunendar, H.; Widiyantoro, S.; Wiyono, S.H.; Hakim, A.; Muhari, A.; et al. Source model for the tsunami inside Palu Bay following the 2018 Palu earthquake, Indonesia. *Geophys. Res. Lett.* **2019**, *46*, 8721–8730. [[CrossRef](#)]
7. Mason, H.B.; Montgomery, J.; Gallant, A.P.; Hutabarat, D.; Reed, A.N.; Wartman, J.; Irsyam, M.; Simatupang, P.T.; Alatas, I.M.; Prakoso, W.A.; et al. East Palu Valley flowslides induced by the 2018 MW 7.5 Palu-Donggala earthquake. *Geomorphology* **2021**, *373*, 107482. [[CrossRef](#)]
8. Syamsidik; Benazir; Muksin, U.; Margaglio, G.; Fitrayansyah, A. Post-tsunami Survey after the September 28, 2018 Tsunami Near Palu Bay of Central Sulawesi, Indonesia: Impacts and Challenges to Coastal Communities. *Int. J. Disaster Risk Reduct.* **2019**, *38*, 101229. [[CrossRef](#)]
9. Luthfi, M. Assessment on Damages of Harbor Complexes Due to Impacts of the 2018 Palu-Donggala Tsunami, Indonesia. In *International Conference on Asian and Pacific Coasts*; Springer: Singapore, 2019; pp. 257–260.
10. Takagi, H.; Pratama, M.B.; Kurobe, S.; Esteban, M.; Aránguiz, R.; Ke, B. Analysis of Generation and Arrival Time of Landslide Tsunami to Palu City Due to the 2018 Sulawesi Earthquake. *Landslides* **2019**, *16*, 983–991. [[CrossRef](#)]
11. Pakoksung, K.; Suppasri, A.; Imamura, F.; Athanasius, C.; Omang, A.; Muhari, A. Simulation of the Submarine Landslide Tsunami on 28 September 2018 in Palu Bay, Sulawesi Island, Indonesia, Using a Two-layer Model. *Pure Appl. Geophys.* **2019**, *176*, 3323–3350. [[CrossRef](#)]
12. Heidarzadeh, M.; Muhari, A.; Wijanarto, B. Insights on the Source of the 28 September 2018 Sulawesi Tsunami, Indonesia Based on Spectral Analyses and Numerical Simulations. *Pure Appl. Geophys.* **2019**, *176*, 25–43. [[CrossRef](#)]
13. Muhari, A.; Imamura, F.; Arikawa, T.; Hakim, A.R.; Afriyanto, F. Solving the Puzzle of the September 2018 Palu, Indonesia, Tsunami Mystery: Clues from the Tsunami Waveform and the Initial Field Survey Data. *J. Disaster Res.* **2018**, *13*. [[CrossRef](#)]
14. Liu, P.L.F.; Higuera, P.; Husrin, S.; Prasetya, G.S.; Prihantono, J.; Diastomo, H.; Pryambodo, D.G.; Susmoro, H. Coastal Landslides in Palu Bay during 2018 Sulawesi Earthquake and Tsunami. *Landslides* **2020**, *17*, 2085–2098. [[CrossRef](#)]
15. Nakata, K.; Katsumata, A.; Muhari, A. Submarine Landslide Source Models Consistent with Multiple Tsunami Records of the 2018 Palu Tsunami, Sulawesi, Indonesia. *Earth Planets Space* **2020**, *72*, 1–16. [[CrossRef](#)]
16. Weatherall, P.; Marks, K.M.; Jakobsson, M.; Schmitt, T.; Tani, S.; Arndt, J.E.; Rovere, M.; Chayes, D.; Ferrini, V.; Wigley, R. A New Digital Bathymetric Model of the World's Oceans. *Earth Space Sci.* **2015**, *2*, 331–345. [[CrossRef](#)]
17. HydroQual, Inc. *A Primer for ECOMSED, Users Manual (Version 1.3)*; HydroQual, Inc.: Mahwah, NJ, USA, 2002; p. 07430.
18. Lai, Y.G.; Wu, K. A Three-Dimensional Flow and Sediment Transport Model for Free-Surface Open Channel Flows on Unstructured Flexible Meshes. *Fluids* **2019**, *4*, 18. [[CrossRef](#)]
19. Mellor, G.L. *Users Guide for a Three Dimensional, Primitive Equation, Numerical Ocean Model*; Program in Atmospheric and Oceanic Sciences, Princeton University: Princeton, NJ, USA, 1998.
20. Seo, H.; Miller, A.J.; Norris, J.R. Eddy–wind Interaction in the California Current System: Dynamics and impacts. *J. Phys. Oceanogr.* **2016**, *46*, 439–459. [[CrossRef](#)]
21. Khoirunnisa, H.; Karima, S. The Condition of Significant Wave Height and Wind Velocity in Makassar Strait During 2017. *J. Appl. Geospat. Inf.* **2019**, *3*, 179–189. [[CrossRef](#)]
22. BMKG. *Buletin Cuaca dan Iklim Maritim*; BMKG: Jakarta, Indonesia, 2018; Volume 2, p. 20. (In Indonesian)
23. Longuet-Higgins, M.S.; Stewart, R.W. Changes in the Form of Short Gravity Waves on Long Waves and Tidal Currents. *J. Fluid Mech.* **1960**, *8*, 565–583. [[CrossRef](#)]

24. Echevarria, E.R.; Hemer, M.A.; Holbrook, N.J. Global Implications of Surface Current Modulation of the Wind-wave Field. *Ocean Model.* **2021**, *161*, 101792. [[CrossRef](#)]
25. Davarpanah Jazi, S.; Wells, M.G.; Peakall, J.; Dorrell, R.M.; Thomas, R.E.; Keevil, G.M.; Darby, S.E.; Sommeria, J.; Viboud, S.; Valran, T. Influence of Coriolis Force Upon Bottom Boundary Layers in a Large-scale Gravity Current Experiment: Implications for Evolution of Sinuous Deep-water Channel Systems. *J. Geophys. Res. Ocean.* **2020**, *125*, e2019JC015284. [[CrossRef](#)]
26. Bressan, A.; Constantin, A. The Deflection Angle of Surface Ocean Currents from the Wind Direction. *J. Geophys. Res. Ocean.* **2019**, *124*, 7412–7420. [[CrossRef](#)]
27. Boyd, J.P. *Dynamics of the Equatorial Ocean*; Springer: Berlin/Heidelberg, Germany, 2018.
28. Pudjaprasetya, S.R.; Risriani, V.M.; Iryanto. Numerical Simulation of Propagation and Run-Up of Long Waves in U-Shaped Bays. *Fluids* **2021**, *6*, 146. [[CrossRef](#)]
29. Lutfi, M. Three Dimensional Numerical Modeling of Current and Temperature Distribution in the Estuary of Palu River. *J. Phys. Conf. Ser.* **2019**, *1354*, 012020. [[CrossRef](#)]
30. Bayhaqi, A.; Wissha, U.J.; Surinati, D. Modeling Tidal Current of Banten Bay during Transitional Monsoons 2015–2016. *J. Segara* **2018**, *14*, 95–105.
31. Pamungkas, A.; Farhaby, M.A. Hydro-Oceanography Modelling Characteristic (Tides, Waves, and Currents) in Kelabat Bay, Bangka Belitung. In Proceedings of the International Conference on Maritime and Archipelago (ICoMA 2018), Bangka Belitung, Indonesia, 13–15 September 2019; pp. 178–182.
32. Lin, H.; Chen, Z.; Hu, J.; Cucco, A.; Zhu, J.; Sun, Z.; Huang, L. Numerical simulation of the Hydrodynamics and Water Exchange in Sansha Bay. *Ocean Eng.* **2017**, *139*, 85–94. [[CrossRef](#)]
33. Anugrah, N.N.; Samad, W.; Berlianty, D. The Changes in Oceanographic Condition of Makassar Strait Related with El Nino Southern Oscillation (ENSO) Events of 2009–2019. In *IOP Conference Series: Earth and Environmental Science*; IOP Publishing: Bristol, UK, 2020; Volume 618, p. 012017.
34. Sprintall, J.; Wijffels, S.E.; Molcard, R.; Jaya, I. Direct Estimates of the Indonesian Throughflow Entering the Indian Ocean: 2004–2006. *J. Geophys. Res. Ocean.* **2009**, *114*, 2004–2006.
35. Gordon, A.L.; Susanto, R.D.; Field, A.; Huber, B.A.; Pranowo, W.; Wirasantosa, S. Makassar Strait Throughflow, 2004 to 2006. *Geophys. Res. Lett.* **2008**, *35*, 3–7. [[CrossRef](#)]
36. Qu, T.; Song, Y.T.; Yamagata, T. An introduction to the South China Sea Throughflow: Its Dynamics, Variability, and Application for Climate. *Dyn. Atmos. Oceans* **2009**, *47*, 3–14. [[CrossRef](#)]
37. Mayer, B.; Damm, P.E. The Makassar Strait Throughflow and Its jet. *J. Geophys. Res. Oceans* **2012**, *117*, C7. [[CrossRef](#)]
38. Lutfi, M. Hydrodynamics Circulation Model in the Estuary of Palu River Based on Numerical Calculations. *J. Eng. Sci. Technol.* **2020**, *15*, 2309–2323.
39. Radjawane, I.M.; Riandini, F. Numerical Simulation of Cohesive Sediment Transport in Jakarta Bay. *Int. J. Remote Sens. Earth Sci.* **2009**, *6*, 65–76. [[CrossRef](#)]
40. Mishima, T.; Yamashita, T.; Komaguti, T.; Riandini, F. Application of Simulation Model for Cohesive Sediment Transport and Bottom Topography Changes to Tidal Flat. *Proc. Hydraul. Eng.* **2008**, *52*, 1333–1338. [[CrossRef](#)]
41. Choi, B.H.; Eum, H.M.; Woo, S.B. Modeling of Coupled Tide-wave-surge Process in the Yellow Sea. *Ocean Eng.* **2003**, *30*, 739–759. [[CrossRef](#)]
42. Cossa, O.; Pous, S.; Penven, P.; Capet, X.; Reason, C.J.C. Modelling Cyclonic Eddies in the Delagoa Bight Region. *Cont. Shelf Res.* **2016**, *119*, 14–29. [[CrossRef](#)]
43. Johnson, J.A.; Hill, R.B. A Three-dimensional Model of the Southern Ocean with Bottom Topography. *Deep-Sea Res. Oceanogr. Abstr.* **1975**, *22*, 745–751. [[CrossRef](#)]